

The Correlation of Gamma-Ray Bursts with Active Galactic Nuclei.

R. A. Burenin, A. A. Vikhlinin, O. V. Terekhov, and S. Yu. Sazonov

*Space Research Institute, Russian Academy of Sciences
Profsoyuznaya 84/32, 117810 Moscow, Russia*

Abstract

We search for angular correlation of gamma-ray bursts with cataloged quasars, BL Lac objects, and AGN using a large sample of relatively well-localized bursts detected by WATCH on board GRANAT and EURECA, IPN, and BATSE (327 bursts total). A statistically significant (99.99% confidence) correlation between GRB and $M_B < -21$ AGN in the redshift range $0.1 < z < 0.32$ is found. The correlation with AGN is detected, with a lower significance, in three independent GRB datasets. The correlation amplitude implies that, depending on the AGN catalog completeness, 10% to 100% of bursts with peak fluxes in the range $3 - 30 \times 10^{-6}$ erg s $^{-1}$ cm $^{-2}$ in the 100–500 keV band are physically related to AGN. The established distance scale corresponds to the energy release of order 10^{52} ergs per burst.

1 Introduction

Gamma-ray bursts are distributed isotropically on the sky; their peak flux distribution shows the lack of faint bursts compared to the expectation for a homogeneous distribution in Euclidean space (see e.g. Fishman & Meegan 1995 for review). These observed properties of GRB are reproduced by two popular models: 1) GRB arise in an extended Galactic halo with a core radius of ~ 100 kpc and 2) GRB are located at cosmological distances.

The Galactic halo models are challenged by the observed isotropy of the burst positions. The isotropy constraints much improved recently, and as a result, most variants of the halo model are no longer viable (Briggs et al. 1996). An additional argument against the Galactic halo model comes from *Einstein* data. The *Einstein* IPC sensitivity is sufficient to detect bursts from the halos of nearby galaxies, but they were not found in the data (Hamilton et al. 1996).

In the cosmological model, the burst isotropy and departures of $\log N - \log S$ from the Euclidean $S^{-3/2}$ law are explained naturally. The minimum redshift $z = 0.835$ of the optical transient associated with GRB 970528 (Metzger et al. 1997) is a decisive evidence in favor of the cosmological model. Optical spectroscopy of the GRB counterparts is complicated by the faintness of associated optical

transients and their relatively featureless spectrum (e.g., no strong emission lines were observed in the GRB 970528 optical transient). Therefore, indirect estimates of the GRB distance scale are still useful.

The shape of the GRB peak flux distribution implies that sources of the dimmest BATSE bursts are at $z \sim 1$, assuming no source evolution (Emslie & Horack 1994; Fishman & Meegan 1995 and references therein). For some plausible evolution of GRB volume density, the above distance estimate can vary by a factor of $\gtrsim 2$ (Horack et al. 1995). Using a different approach, Quashnock (1996) derived $z > 0.25$ for the dimmest BATSE bursts by cross-correlating the third BATSE catalog with the known large scale structure at low redshifts.

Some earlier studies already searched for a direct relationship between GRB and other astrophysical objects at cosmological distances. Kolatt & Piran (1996) and Marani et al. (1997) found that GRB from the third BATSE catalog are correlated with Abell clusters. However, using more precise GRB localizations, Burenin et al. (1997), Hurley et al. (1997), and Gorosabel & Castro-Tirado (1997) have not found any correlation with Abell clusters. Furthermore, the amplitude of correlation of well-localized GRB and $z < 0.1$ Abell clusters is lower than expected in the case of the same spatial distribution of GRB and optically luminous matter (Bu-

renin et al. 1997). If this result is interpreted as an indication that bright and well-localized GRB are at greater distances than nearby Abell clusters, the dimmest BATSE bursts should be at $z > 0.3$, in agreement with Quashnock's (1996) results.

At still higher redshifts, $z \sim 0.1 - 1$, a natural choice is to search for correlation of GRB with quasars and other flavors of active galactic nuclei, which comprise the majority of known objects at these high redshifts. To search for correlation of AGN and GRB is also attractive because some theoretical models relate bursts to physical processes in active nuclei (e.g. Lejter 1980, Carter 1992). Some attempts to search for such a correlation have been undertaken earlier. A marginal evidence for excess of QSO in the small Interplanetary Network (IPN) GRB error boxes has been found (Vrba et al. 1995). However, Webber et al. (1995) and Gorosabel et al. (1995) found that the number of QSO and AGN in GRB error boxes is consistent with random. These earlier analyses were based on a smaller number of bursts with good localizations than available at present. Citing a recent work, Schartel et al. (1997) have found a correlation of well-localized GRB from the third BATSE catalog with radio-quiet QSO. The strongest correlation was detected at the $> 99.7\%$ confidence level for intrinsically bright QSO with $z < 1$.

The goal of this work is to search for a correlation of GRB with QSO and AGN using all available data for good, with $\lesssim 1^\circ$ uncertainty, bursts localizations. We use $H_0 = 50 \text{ km s}^{-1} \text{ Mpc}^{-1}$ and $q_0 = 0$.

2 The data

2.1 Bursts localizations

We use 327 published gamma-ray bursts with positions known to better than $\sim 1^\circ$. We divide all bursts in three sets basing on the origin of the burst position measurement. The first set includes 43 burst positions measured by WATCH/GRANAT (Sazonov et al. 1998), 12 — by WATCH/EURECA (Brandt et al. 1995), 30 — by IPN 78–80 (Atteia et al. 1987). Thirteen more localizations were found in the literature cited by Lund (1995). All these sources provide 99% confidence burst position regions. In total, the first set contains 98 bursts.

The second and third data sets are based on BATSE data. We use only bursts with BATSE error circle $< 1.8^\circ$ at 68% confidence. The second data set includes 117 such bursts from the third BATSE catalog (Meegan et al. 1996), excluding those GRB which are already in the first set. The third data set

includes 112 bursts from the current BATSE catalog, excluding bursts already in the first or second sets. The current catalog was download on October 13, 1997 from <http://www.batse.msfc.nasa.gov/>.

Peak fluxes of the GRB in use are in the range $\sim 3 - 30 \times 10^{-6} \text{ erg s}^{-1} \text{ cm}^{-2}$ in the 100–500 keV energy band; the peak fluxes, and hence the burst distance distributions, are approximately the same in all three datasets.

2.2 Catalog of QSO and AGN

We used QSO and AGN from Véron-Cetty & Véron (1996; VCV96 hereafter) “Catalogue of Quasars and Active Nuclei” compiled from the literature. This catalog contains 8609 QSO, 220 BL Lac objects, and 2833 AGN. The catalog completeness varies with the object class and redshift which makes a secondary selection warranted. Since we have only 327 GRB, it is meaningless to correlate their positions with objects from a catalog with completeness $< 0.3\%$. We attempted to define subsamples of VCV96 catalog which are complete at the level sufficient to search for angular correlation of objects and GRB.

Figure 1 shows number density of QSO from VCV96 as a function of redshift. The distribution predicted for the pure luminosity evolution model of Franceschini et al. (1994) is also shown. It is clear that VCV96 catalog of QSO is almost complete at $z < 0.1$; it is less than 0.3% complete at $z > 1$ and it is meaningless to search for correlation of our GRB and QSO at this redshift. Similarly, we find that the catalog becomes essentially incomplete for BL Lac objects at $z \gtrsim 0.3$ and for AGN already at $z \sim 0.03$ (Fig. 2). As was discussed in §1, sources of bright bursts are probably located at higher redshifts, $z \sim 0.1 - 1$, therefore the search for correlation of GRB and all AGN from VCV96 can be inconclusive. The subsample of intrinsically luminous AGN, $M_B < -21$, is more complete at high redshifts. The solid line in Fig. 2 shows the redshift distribution $M_B < -21$ AGN. We also show the number densities expected from AGN luminosity functions in Hamburg/ESO (HES, Köhler et al. 1997) and the Large Bright Quasar (LBQS, Hewett et al. 1993) surveys. It is clear from Fig. 2 that VCV96 catalog is reasonably complete for $M_B < -21$ AGN out to $z \sim 0.3$. We will search for correlation of GRB with these luminous AGN.

3 Data analysis

A naive method to search for correlation of objects and GRB would be to count the number of ob-

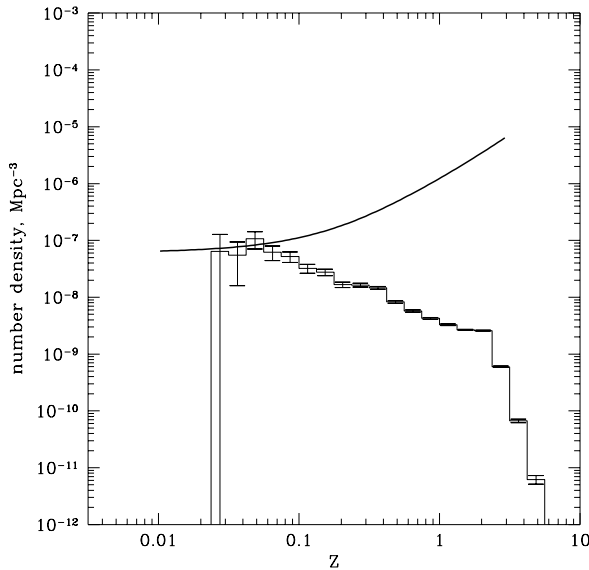


Fig. 1— Number density of QSO from VCV96 as a function of redshift. Smooth solid line represents the true number density of these objects (accounting for their cosmological evolution, Franceschini et al. 1994).

jects inside the GRB position error boxes and compare this number with that expected for random burst/object locations. However, the spatial distribution of AGN and QSO from the VCV96 catalog is very non-uniform, because many objects were found in deep, small area surveys. In this case, it is better to use a statistic, which we denote δ , of the number of bursts whose position error regions contain at least one AGN or QSO. The distribution of δ expected for purely chance associations can be derived by Monte-Carlo simulations in which the actual AGN and QSO catalog is cross-correlated with mock catalogs of randomly located GRB. The mock GRB catalogs were simulated with the same position error boxes as in the data, but with centroid positions distributed randomly. In simulating GRB positions, we accounted for the sky exposure for WATCH/GRANAT and BATSE bursts, and assumed a uniform coverage for other experiments. We have found that the distribution of δ derived from simulations is accurately approximated by the binomial distribution with the number of trials, n , equal to the number of bursts, and success probability $p = \langle \delta \rangle / n$, where $\langle \delta \rangle$ is the average value derived from simulations. This binomial approximation was used to estimate the probability of strong deviations of δ found in our analysis.

In search for angular correlation, it is reasonable

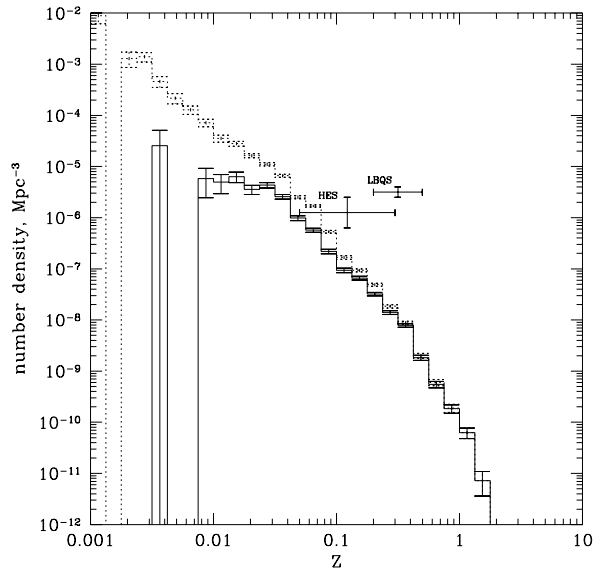


Fig. 2— Number density of AGN from VCV96 as a function of their redshift. Dotted histogram represents number density of all AGN, the solid one corresponds to bright $M_B < -21$ AGN.

to restrict the AGN redshift range since there are indications that the GRB luminosity function must be narrow, $\Delta \lg L \approx 1$ (Emslie & Horack 1994). If this is the case, the flux range of our bursts corresponds to the distance range of a factor of $\lesssim 10$. Therefore, the sensitivity can be enhanced by considering only AGN with $0.1z_{\lim} < z < z_{\lim}$ and varying z_{\lim} . The sensitivity may be enhanced still further if the lower boundary is a larger fraction of z_{\lim} , because the VCV96 catalog completeness falls rapidly with redshift, while most of the volume (and presumably, most of the GRB sources) is near the upper boundary of the redshift interval. Therefore, we use the redshift range $0.32z_{\lim} < z < z_{\lim}$. In doing so, we retain approximately 97% of the volume of the original $0.1z_{\lim} < z < z_{\lim}$ interval and in the same time significantly improve the sensitivity.

4 Results

As a first step, we performed the correlation analysis for QSO, BL Lac objects, and bright AGN without any redshift constraints. The results are presented in Table 1, where we list the observed values of δ (recall that δ is the number of bursts with at least one catalogued object inside the error box), the average values $\langle \delta \rangle$ expected for purely chance associations of bursts and objects, and the probability to find a larger value of δ than observed. In nei-

Table 1 — Correlation analysis without redshift constraints

	Number of bursts	$\langle \delta \rangle$	δ_0	$P(\delta \geq \delta_0), \%$
QSO (8609 objects):				
dataset #1	98	9.41	13	15.6
dataset #2	117	46.26	55	9.9
dataset #3	112	44.31	47	34.3
all	327	96.02	115	2.6
BL Lac (220 objects):				
dataset #1	98	0.66	2	14.2
dataset #2	117	5.50	2	97.4
dataset #3	112	5.04	2	96.1
all	327	11.19	6	96.4
Bright AGN (1390 objects):				
dataset #1	98	3.38	6	12.7
dataset #2	117	22.26	26	21.4
dataset #3	112	20.94	25	18.7
all	327	45.92	57	5.1

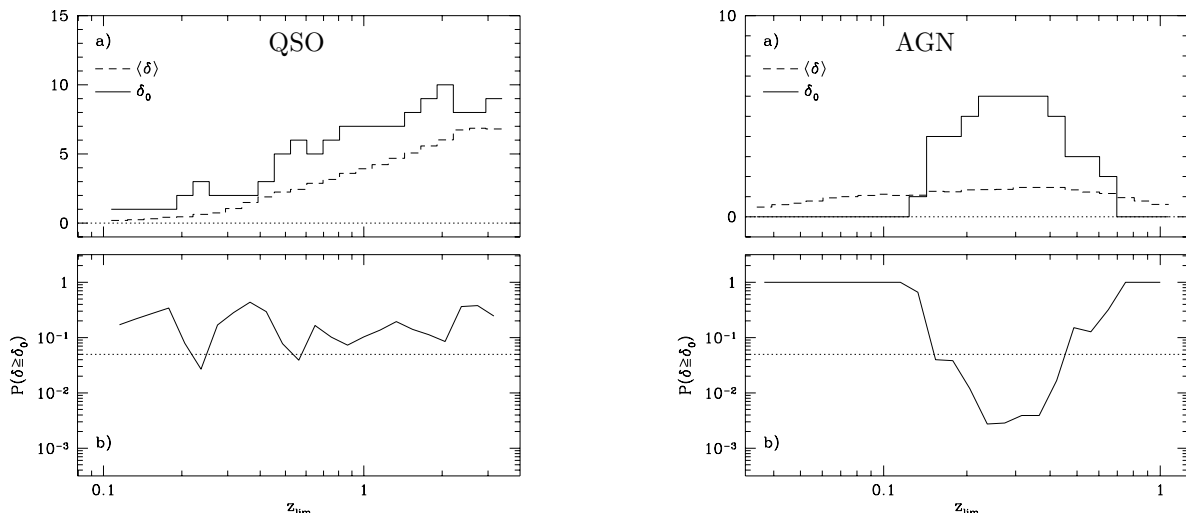


Fig. 3 — Correlation analysis of the first GRB dataset with the QSO and AGN. Solid lines in the upper panels show the values of δ (see text) found in the data with the redshift constraint $0.32z_{\text{lim}} < z < z_{\text{lim}}$ applied. The dashed lines in the upper panel show the expected values of δ for a purely random position association between GRB and QSO/AGNs. The lower panels show the probability of producing the observed δ 's from random fluctuations. The dotted line in the lower panels show the 95% (2σ) significance level.

ther case, a significant (at at least 99% confidence) correlation is found.

Next, we performed the correlation analysis with the redshift constraints as described in §3 above. In particular, we considered QSO or AGN¹ in the redshift interval $0.32z_{\text{lim}} < z < z_{\text{lim}}$, and determined the values δ_0 , $\langle \delta \rangle$, and $P(\delta > \delta_0)$ as a function of limiting redshift z_{lim} . Results for the first

GRB dataset are shown in Fig. 3 for both QSO and AGN. While QSO show a slight excess of δ over random expectations, this excess is $< 2\sigma$ significant at almost all z_{lim} . AGN, on the contrary, show a profound peak of correlation for $z_{\text{lim}} \sim 0.3$, i.e. in the redshift interval $0.1 \lesssim z \lesssim 0.3$. The excess of the observed value of δ over $\langle \delta \rangle$ is significant at the 99.8% confidence.

¹The number of BL Lac objects in the VCV96 catalog is too small to analyze different redshift intervals separately, so we do not consider them below.

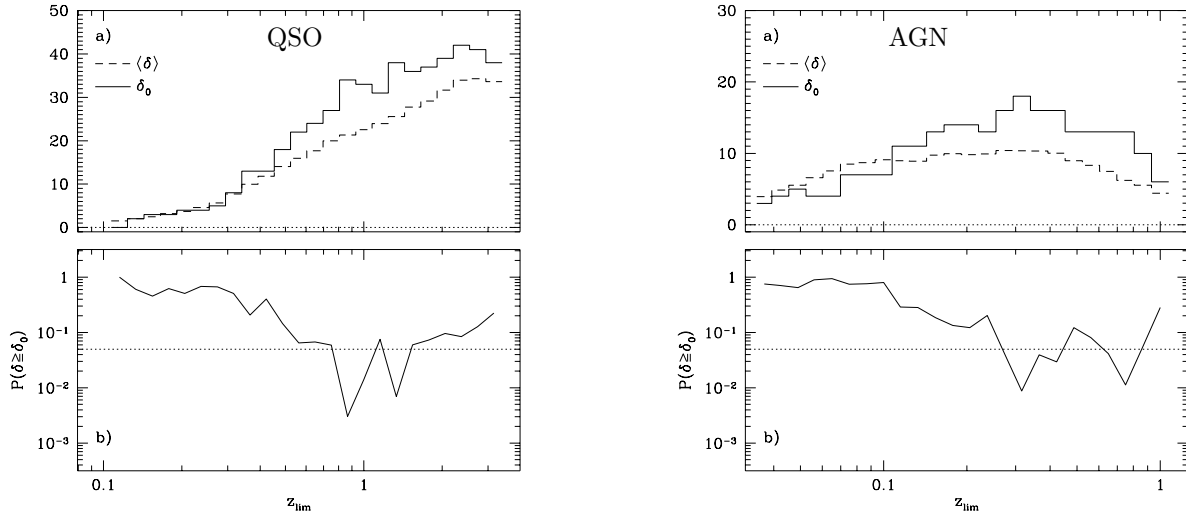


Fig. 4 — Same as Fig. 3, but for the second GRB dataset (the third BATSE catalog).

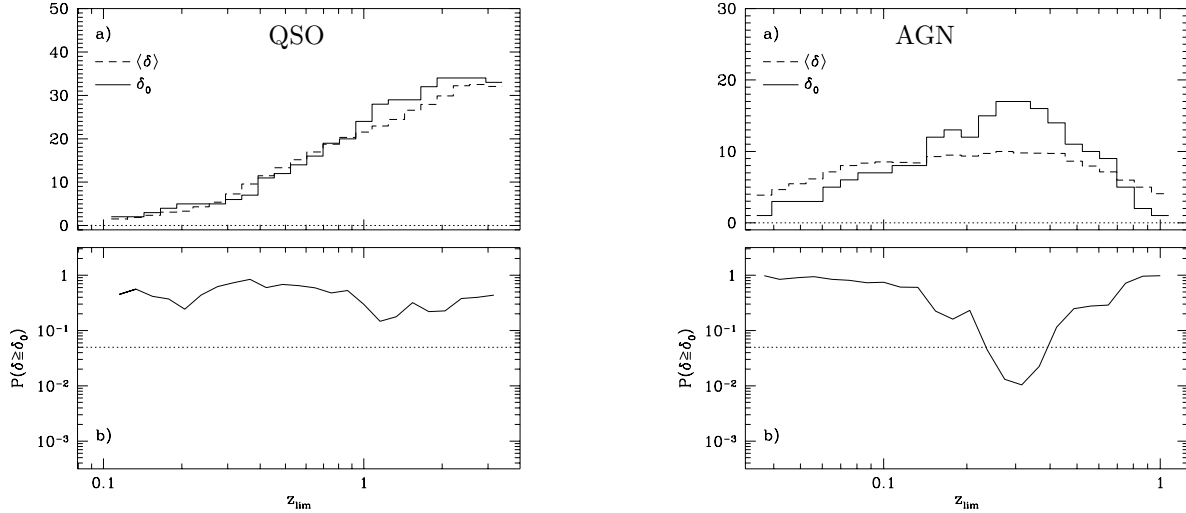


Fig. 5 — Same as Fig. 3, but for the third GRB dataset (the current BATSE catalog).

The results for 117 bursts from the second GRB dataset (the third BATSE catalog), 112 bursts from the third GRB dataset (the current BATSE catalog), and all three datasets combined (327 bursts in total) are shown in Figs. 4, 5, and 6, respectively. The peak of the GRB-AGN correlation amplitude at $z_{\text{lim}} \approx 0.3$ found in the first dataset, is present in two other datasets. When all three GRB datasets are combined (Fig. 6), the statistical significance of this correlation is very high, 99.9985%. Of course, the AGN redshift range was optimized, therefore the actual significance is somewhat lower. The number of independent redshift intervals in our analysis can be estimated as the ratio of the log width of the searched redshift range $0.03 < z < 1$ and the log width of individual intervals $\Delta \lg z \approx 0.5$. Allowing for the partial overlap, we find ~ 10 independent redshift “trials”, and hence the actual significance of the correlation is $\sim 99.985\%$.

Gamma-ray bursts from the second dataset show some correlation with QSO with a $\sim 99.7\%$ significance (Fig. 4). It is this correlation that was found by Schartel et al. (1997). However, this correlation is absent in two other datasets (Fig. 3 and Fig. 5); hence, the GRB-QSO correlation in Fig. 4 probably can be explained by a random deviation.

We conclude that the most prominent correla-

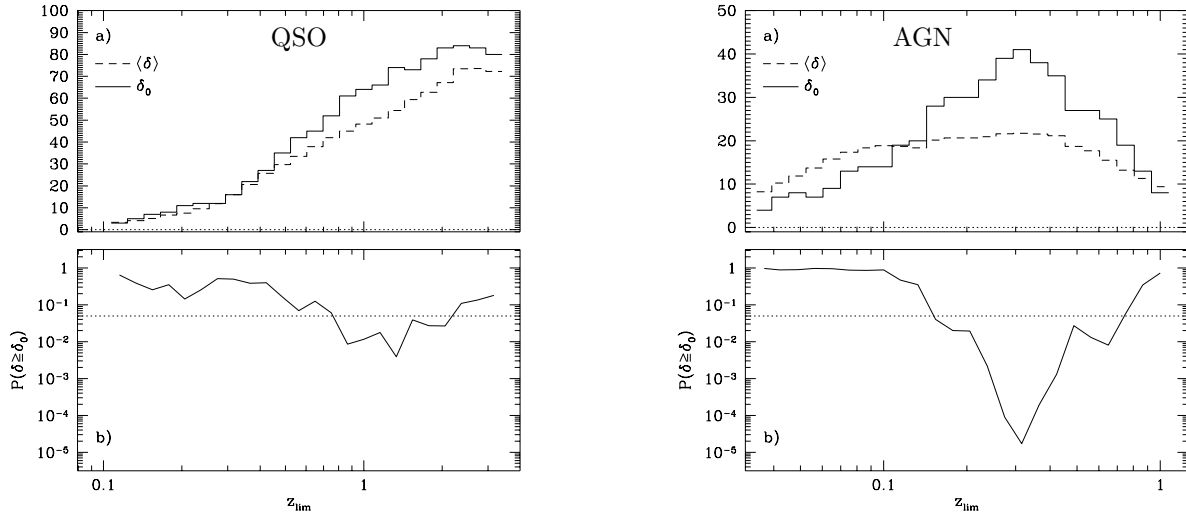


Fig. 6 — Same as Fig. 3, but for all three GRB datasets (327 bursts in total).

tion of gamma-ray bursts with extragalactic objects found so far is that with the Active Galactic Nuclei in the redshift range $0.1 \lesssim z \lesssim 0.3$. This correlation suggests that at least some bursts may be physically related to AGN. Next, we want to determine the fraction of bursts related to AGN in the redshift interval $0.1 < z < 0.32$. Since not all AGN in this interval are cataloged, we first estimated the fraction of bursts which may be related to AGN *from the VCV96 catalog*. To derive the fraction of bursts which may be related to *both cataloged and not cataloged* AGN, this fraction must be divided by the catalog completeness.

The fraction of bursts originating in cataloged AGN, f_b , has been estimated as follows. Given f_b , the number of physically connected bursts, n_b , was drawn from the binomial distribution with success probability f_b and the number of trials equal to the number of bursts. We then randomly picked n_b AGN and n_b bursts from the data, and set burst error region centroids at the chosen AGN. The positions for the rest of GRB were chosen randomly, as in §3. We then found the value of δ for such a mock burst catalog. Repeating these simulations, we derived the probability distribution $P(\delta)$ as a function of f_b . Using the derived $P(\delta, f_b)$ we estimated the best-fit f_b as a value which maximized the probability to obtain the observed value δ_0 , i.e. which minimized $C = -2 \log L = -2 \log P(\delta_0, f_b)$. Here C is equivalent to the C-statistics of Cash (1979), and so the confidence intervals of f_b can be derived from the change in C .

This analysis was performed separately for BATSE (second+third datasets) and non-BATSE

(first dataset) burst data. In the case of BATSE data with 68% position error circles, the derived value f_b has been corrected by a factor of 1.47. For both BATSE and non-BATSE data, we obtained consistent fractions, of order of several percent, of bursts originating in the cataloged AGN. For the first dataset, $f_b = 0.040^{+0.025}_{-0.023}$ (68%) and $^{+0.055}_{-0.036}$ (95% confidence). For the bursts detected by BATSE (second and third data sets together): $f_b = 0.098^{+0.037}_{-0.038}$ (68%) and $^{+0.080}_{-0.070}$ (95%).

Next, we have to correct f_b for the incompleteness of the VCV96 catalog. If one assumes that at $z < 0.03$, all $M_B < -21$ AGN are cataloged, the completeness in the $0.1 < z < 0.32$ interval is low, 0.007. If, instead, the HES survey luminosity function is used, the completeness is ~ 0.03 . Both these values are smaller than the estimated f_b , which means, formally, that more than 100% of bursts originate in AGN. Clearly, this is unphysical, and we discuss some possible explanations below. Nevertheless, similar values of f_b and catalog completeness suggest that a very significant fraction of GRB is related to AGN. Below we discuss this result in connection with previous attempts to identify optical counterparts of gamma-ray bursts.

5 Discussion

This is not the first attempt to find optical counterparts of GRB by analyzing the optical content of small-area localizations, so the comparison of our results with some previous works is in order.

Vrba et al. (1995) have performed extensive optical photometry of 8 small-area ($< 70 \text{ arcmin}^2$)

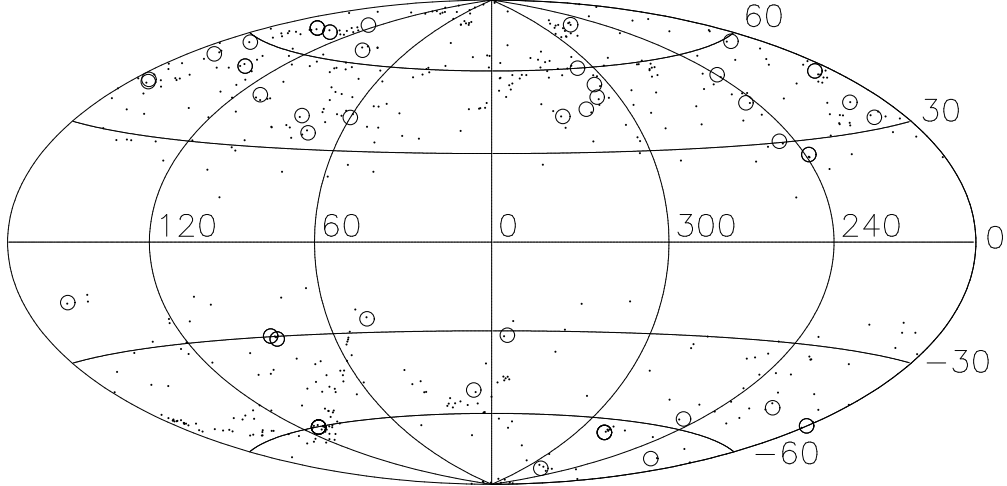


Fig. 7 — The distribution of $0.1 < z < 0.32$ AGN from the VCV96 catalog in Galactic coordinates. Circles mark positions of GRB which have at least one AGN within the position error region.

IPN localizations searching for objects with unusual colors, variability, and proper motions. Only blue objects, which Vrba et al. interpreted as QSO, showed a marginal excess at a rate approximately one per localization. This is in agreement with our results.

Webber et al. (1995) and Gorosabel et al. (1995) used several tens GRB localizations from IPN and WATCH, respectively. The optical content was taken from existing catalogs, similar to our study. No excess of either AGN or any other class of objects was found. These results do not directly contradict to ours because Webber et al. (1995) and Gorosabel et al. (1995) used a smaller number of bursts, did not account for the incompleteness of optical catalogs (§2.2), and did not apply redshift constraints in search for correlation. Since the completeness of the VCV96 catalog (and probably other all-sky catalogs) is below, or on the level of, several percent (§4), analyses based on several tens of bursts are inconclusive.

The most similar to ours is the work of Schartel et al. (1997) who cross-correlated BATSE bursts with the AGN and QSO from VCV96. They found a marginal correlation with QSO, and no correlation with AGN, with no redshift constraints applied to AGN. We essentially reproduce these results (Fig. 4 and Table 1). A significant correlation with AGN found in our analysis is not found by Schartel et al. because they used a smaller number of bursts, with poorer localizations (only BATSE data), and used the entire VCV96 catalog which is very incomplete for AGN even at low redshift (§2.2).

Finally, we mention the two GRB with small-

area localizations, in which AGN were found. Drinkwater et al. (1997) report that the possible X-ray counterpart of GRB 920501 is associated with a Seyfert 1 galaxy at $z = 0.315$. The first X-ray localization of a gamma-ray burst by BeppoSAX (3' radius) contains a $z = 1.038$ QSO (Piro et al. 1998). On the other hand, optical transients associated with other BeppoSAX bursts, GRB 970508, 970228, and 971214 probably are not AGN.

Our analysis supersedes most of earlier searches for GRB-AGN association because we used a large GRB dataset, carefully accounted for incompleteness of the optical catalogs, and introduced sensible object redshift constraints. These advantages made it possible to find the strongest ever evidence for association of GRB with a known class of extragalactic objects. However, there are several problems with our analysis. First, we used relatively large area gamma-ray burst localizations, and therefore had to perform a statistical correlation rather than an object-by-object identification. Second, we used a sparse catalog of AGN and QSO, in which many objects were found in a number of small-area high-sensitivity searches. In fact, this introduces a possibility that the correlation we detect is not with AGN but rather with objects around which the AGN we searched, e.g. normal galaxies or other QSO (data from Arp 1980 and Monk et al. 1988), targets of *Einstein* pointings (EMSS AGN, Stocke et al. 1991). However, the sky distribution of GRB with $0.1 < z < 0.32$ AGN inside the localization area, does not generally follow the regions of deep AGN surveys (Fig. 7). Also, a clear redshift dependence of the correlation is not easily explainable in

such a scenario.

Another problem is that the amplitude of the detected correlation implies that the fraction of bursts related to AGN is somewhat higher than the estimated completeness of the optical catalog (§4). We can offer two possible explanations. First is that GRB prefer luminous AGN, for which the catalog completeness is higher. Second is that GRB prefer a certain type of AGN (Seyfert 1 or 2, X-ray loud or quiet, radio loud or quiet, etc.) which is more commonly present in the VCV96 catalog than the “average” AGN.

Despite these problems, we believe that the case for an association of bright gamma-ray bursts with AGN at moderate redshift is compelling. This case can be further proved, or disproved, by an extensive optical, preferably spectroscopic, survey of small-area localizations of bright GRB, similar to the work of Vrba et al. (1995) but using a larger number of bursts. Another approach would be to use a more complete catalog of AGN covering a significant fraction of the sky; unfortunately, this seems impractical until the Sloan Digitized Sky Survey is completed.

References

Arp, H. 1980, *ApJ*, 240, 415
 Atteia, J.-L., Barat C., & Hurley, K. 1987, *ApJS*, 64, 305
 Brandt, S., Lund, N., & Castro-Tirado, A., J. 1995, *Adv. Space Res.*, 16, 843
 Briggs, M. S. et al. 1996, *ApJ*, 459, 40
 Burenin, R. A., Terekhov, O. V., Sunyaev, R. A., & Sazonov, S. Yu. 1997, *Astronomy Letters*, 23, 768.
 Carter, B. 1992, *ApJ*, 391, L67
 Cash, W. 1979, *ApJ*, 228, 939
 Drinkwater, M. J., Jones, L. A., Blaes, O. M., Hurt, T., Antonucci, R., & Hurley, K. 1997, *IAU Circular* 6600.
 Emslie, A. G. & Horack J. M. 1994, *ApJ*, 435, 16
 Franceschini, A., La Franca, F., Cristiani, S., & Martin-Mirones, J. M. 1994, *MNRAS*, 269, 683
 Gorosabel, J. & Castro-Tirado, A. J. 1997, *ApJ*, 483, L83
 Gorosabel, J., Castro-Tirado, A. J., Lund, N., Brandt, S., Guziy, S., & Shlyapnikov, A. 1995, *Ap&SS*, 231, 297
 Hamilton, T. T., Gotthelf, E. V., & Helfand, D. J. 1996, *ApJ*, 466, 795
 Hurley, K., Hartmann, D., Kouveliotou, C., Fishman, G., Laros, J., Cline, T., & Boer, M. 1997, *ApJ*, 479, L113
 Hewett, P. C., Foltz, C. B., & Chaffee, F. H. 1993, *ApJ*, 406, L43
 Horack, J. M., Emslie, A. G. & Hartmann, D. H. 1995, *ApJ*, 447, 474
 Köhler, T., Groote, D., Reimers, D., & Wisotzki, L. 1997, *A&A*, 325, 520
 Lejter, D. 1980, *A&A*, 89, 370
 Lund, N. 1995, *Ap&SS*, 231, 217
 Meegan, C. A. et al. 1996, *ApJS*, 106, 65
 Metzger, M. R., Djorgovski, S. G., Kulkarni, S. R., Steidel, C. C., Adelberger, K. L., Frail, D. A., Costa, E., & Frontera, F. 1997, *Nature*, 387, 879.
 Monk, A. S., Penston M. V., Pettini M., & Blades, J. C. 1988, *MNRAS*, 234, 193
 Piro, L. et al. 1998, *A&A*, 329, 906
 Quashnock, J. M. 1996, *ApJ*, 461, L69
 Sazonov, S., Sunyaev, R. A., Terekhov, O. V., Lund, N., Brandt, S., & Castro-Tirado, A. J. 1998, *A&AS*, 129, 1
 Schartel, N., Andernach, H., & Greiner, J. 1997, *A&A*, 323, 659
 Stocke, J. T., Morris, S. L., Gioia, I. M., Maccacaro, T., Schild, R., Wolter, A., Fleming, T. A., & Henry, J. P. 1991, *ApJS*, 76, 813
 Véron-Cetty, M. P. & Véron, P. 1996, *ESO Scientific Report*, 17, 1
 Vrba, F. J., Hartmann, D. H., & Jennings, M. C. 1995, *ApJ*, 446, 115
 Webber, W. R., Harrison, T. E., McNamara, B. J., & Lopez, A. 1995, *AJ*, 110, 733

We provide a list of GRB with AGN within localizations. The table lists the experiment in which the burst was localized, burst ID, and names, coordinates (J2000), redshifts and absolute magnitudes of matching AGN.

Note, that due to good localizations of WATCH and IPN bursts, we expect that ~ 4 out of 7 AGN are truly related to bursts (see Fig. 3). For BATSE bursts, which have poorer localizations, we expect that ~ 15 out of 53 AGN are associated with bursts (Fig. 4 and 5).

Table 2 — Gamma-ray bursts with AGN within localizations

Experiment	Burst ID	AGN Name	RA	Dec	z	M_B
W/GR	910627	Q 1313–0153	13 16 24.3	−02 09 45	0.150	−21.6
W/GR	910927	0313–428	03 14 55.9	−42 40 56	0.126	−21.4
W/GR	920210	MS 10185+4830	10 21 38.8	+48 15 10	0.232	−22.1
		Q 1019+4750	10 22 57.0	+47 34 55	0.144	−21.2
W/GR	920720	HE 0936–1058	09 39 11.4	−11 11 46	0.214	−22.4
W/GR	940703	MS 08498+2820	08 52 48.8	+28 08 40	0.197	−21.9
IPN	790101	Q 1215+1545	12 17 32.8	+15 28 45	0.139	−21.7
BATSE	910507	PKS 2004–447	20 07 55.1	−44 34 43	0.238	−21.6
BATSE	911126	Q 1032+062	10 35 06.0	+06 01 41	0.245	−22.2
BATSE	920110	HE 0348–2226	03 50 19.2	−22 17 22	0.111	−22.0
BATSE	920221	Q 1206+4748	12 09 05.9	+47 32 07	0.182	−21.3
		Q 1221+4752	12 23 47.6	+47 35 35	0.307	−21.5
BATSE	920517	IRAS 13305–1739	13 33 16.5	−17 55 00	0.148	−21.2
BATSE	920622	PC 1044+4719	10 47 13.2	+47 03 35	0.247	−21.5
BATSE	921206	Q 1138+4638	11 40 48.2	+46 22 03	0.115	−22.0
		RX J11427+4625	11 42 41.4	+46 24 36	0.114	−22.0
		Q 1145+4638	11 47 47.6	+46 21 46	0.151	−21.1
BATSE	921209	SBS 1116+610	11 19 22.3	+60 48 51	0.298	−22.9
		SBS 1121+606	11 24 17.9	+60 20 26	0.200	−22.5
BATSE	930106	Q 0015+0119	00 17 45.9	+01 36 20	0.236	−22.5
		PB 5853	00 18 22.1	+01 19 01	0.160	−22.8
		Q 0017+0212	00 20 33.2	+02 28 52	0.256	−22.5
		UM 228B	00 21 02.3	+00 52 41	0.142	−22.7
		Q 0019+0022A	00 21 41.0	+00 38 41	0.314	−22.9
		Q 0023+0058	00 26 20.8	+01 15 17	0.274	−22.5
		Q 0023+0228	00 26 21.9	+02 44 42	0.236	−22.4
BATSE	930405	MS 13061–0115	13 08 42.8	−01 31 24	0.111	−21.1
BATSE	930425	0110–361	01 12 32.7	−35 55 35	0.290	−22.0
BATSE	930905	MS 20395–0107	20 42 06.5	−00 56 57	0.142	−21.1
BATSE	931024	E 0906–091	09 08 51.2	−09 18 51	0.129	−21.9
		E 0907–091	09 09 36.2	−09 18 19	0.253	−22.9
BATSE	931204	1631.9+3719	16 33 38.3	+37 13 14	0.115	−21.2
BATSE	940129	MS 08303+2828	08 33 25.9	+28 17 53	0.283	−21.5
BATSE	940704	Q 1400+4638	14 02 08.7	+46 24 13	0.236	−21.8
BATSE	940806	0146–502	01 48 19.5	−50 02 59	0.310	−22.9
		0147–511	01 49 04.4	−50 53 06	0.170	−21.1
		0149–505	01 51 18.5	−50 16 26	0.310	−22.8
		0149–510	01 51 44.6	−50 50 08	0.290	−22.2
BATSE	940830	MS 22229+2046	22 25 19.3	+21 01 45	0.139	−22.3
		MS 22230+2110	22 25 23.9	+21 25 25	0.310	−22.9

Table 2 — *Continued*

Experiment	Burst ID	AGN Name	RA	Dec	z	M_B
BATSE	950305	RX J13113–1411	13 11 18.3	–14 11 28	0.153	–21.4
BATSE	950904	MS 17096+4823	17 10 58.5	+48 19 27	0.174	–22.3
BATSE	951002	PB 6986	03 02 46.8	–02 34 35	0.249	–22.7
		Q 0307–0200	03 10 19.1	–01 48 40	0.207	–22.2
BATSE	951016	PKS 0222–23	02 25 02.6	–23 12 49	0.230	–22.3
BATSE	951102	PG 0906+48	09 10 09.9	+48 13 42	0.118	–22.8
BATSE	951202	A09.64	21 56 03.0	–36 15 15	0.115	–22.2
BATSE	960111	PG 0906+48	09 10 09.9	+48 13 42	0.118	–22.8
BATSE	960206	HE 1254–0934	12 56 56.9	–09 50 16	0.139	–22.2
BATSE	960605	Q 1010–0056	10 13 17.2	–01 10 57	0.202	–22.2
BATSE	960804	RX J14386+6910	14 38 40.7	+69 10 40	0.214	–22.8
BATSE	960807	2E 1028+3102	10 31 39.0	+30 46 46	0.250	–21.5
BATSE	961202	MS 22229+2046	22 25 19.3	+21 01 45	0.139	–22.3
		MS 22230+2110	22 25 23.9	+21 25 25	0.310	–22.9
BATSE	961213	HS 1234+4610	12 36 58.0	+45 53 52	0.240	–22.2
BATSE	970223	NGC 2859 U1	09 24 34.8	+34 40 33	0.230	–21.6
		MS 09227+3420	09 25 46.0	+34 07 46	0.158	–22.2
BATSE	970411	3C 93.1	03 48 46.9	+33 53 16	0.244	–21.9
BATSE	970420	RX J14136–1538	14 13 40.3	–15 38 33	0.226	–22.9
BATSE	971006	2E 1640+5345	16 42 00.8	+53 39 51	0.140	–21.6